NANO LETTERS

pubs.acs.org/NanoLett Letter

In Situ Study of the Ferroelectric−Antiferroelectric Phase Transition in $Hf_{1-x}Zr_xO_2$ at Elevated Temperatures up to 600 °C

Kisoo Nam,[†] Zehao Lin,[†] Tae Ryong Kim, Chang Niu, Sumi Lee, Shengyao Huang, Juanjuan Lu, Chang Liu, Sumeet K. Gupta, Haiyan Wang, and Peide D. Ye*

Cite This: *Nano Lett.* 2026, 26, 6386−6393 Read Online

ACCESS Metrics & More Article Recommendations Supporting Information

ABSTRACT: Ferroelectric (FE) $Hf_{1-x}Zr_xO_2$ (HZO) has emerged as a promising candidate for non-volatile memory applications due to its excellent scalability, CMOS compatibility, and low thermal budget. However, its phase stability under elevated temperature conditions remains insufficiently understood. Here, we present a comprehensive study on the temperature-dependent phase behavior of HZO capacitors up to 600 °C. By systematically varying film thickness and composition, we identify the critical conditions under which the ferroelectric−antiferroelectric (FE−AFE) transition emerges. Experimental results reveal that this transition originates from the thermal stabilization of the tetragonal phase, as confirmed by sublattice phase-field simulations. Thinner films and Zr-rich compositions exhibit lower transition temperatures, while Hf-rich compositions maintain ferroelectricity at higher temperatures. Furthermore, the FE−AFE transition is shown to be both reversible and repeatable under thermal cycling. These findings provide key insights for the co-design of materials, processes, devices, and reliability in the development of CMOS-compatible ferroelectric memory under variable thermal environments.

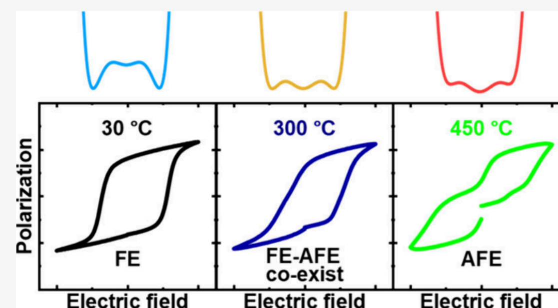

KEYWORDS: *ferroelectric, hafnium oxide, zirconium oxide, phase transition, high temperature*

Ferroelectric (FE) material-based non-volatile memory devices have garnered significant attention due to their high writing speed, excellent endurance, and low energy consumption.[1] Among these materials, $Pb(Zr,Ti)O_3$ (PZT) has been widely commercialized for ferroelectric random-access memory (FeRAM).[2,3] However, the scalability limitations and fatigue issues of PZT have prompted the search for alternative materials.[4] Since the discovery of ferroelectricity in doped HfO_2 in 2011,[5] the excellent scalability and silicon compatibility of doped hafnia have led to extensive research efforts. Various dopants, including Si,[5] Al,[6] Y,[7] La,[8] and Zr,[9] have been explored, with Zr-doped HfO_2 emerging as a particularly promising candidate for memory applications owing to its low thermal budget (≤450 °C).[9,10]

Recent studies have addressed challenges in hafnia-based ferroelectrics, such as fatigue, memory window enhancement, ultrathin ferroelectrics, and novel device architectures.[11−13] However, the thermal stability of $Hf_{0.5}Zr_{0.5}O_2$ (HZO) remains insufficiently understood despite its practical importance.[14] This issue is practically important, as memory devices are often subjected to high-temperature conditions caused by self-heating or operation in harsh environments.[15] Given hafnia's complex phase composition and the marginal energy differences between its phases,[16,17] understanding phase stability under thermal stress is critical for its reliable applications.

The Landau−Devonshire (L−D) framework is commonly employed to analyze switching behavior and phase transitions in FE materials.[18] In HZO, ferroelectricity originates from the orthorhombic (o) phase,[10] which ideally exhibits a global energy minimum and undergoes a second-order transition between two opposite polarization states.[19] However, in practical L−D plots of HZO, the presence of not only the o phase but also the tetragonal (t) phase must be considered, whose presence enables the possibility of a first-order phase transition.[20,21] As illustrated in Figure 1a, the t phase remains metastable at low temperatures and polarization switching occurs directly between the two stable o phase states without involving the t phase. Nevertheless, due to the small symmetry and lattice energy differences between the o and t phases,[22] both phases can become equally stable with increasing temperature, resulting in the coexistence of three global minima. At sufficiently high temperatures, the t phase becomes energetically favorable, leading to pronounced macroscale antiferroelectric (AFE) switching behavior.

Received: February 13, 2026
Revised: April 30, 2026
Accepted: April 30, 2026
Published: May 6, 2026

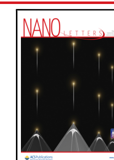

Downloaded via PURDUE UNIV on May 22, 2026 at 16:47:10 (UTC).
See https://pubs.acs.org/sharingguidelines for options on how to legitimately share published articles.

ACS Publications © 2026 American Chemical Society

https://doi.org/10.1021/acs.nanolett.6c00781
Nano Lett. 2026, 26, 6386−6393

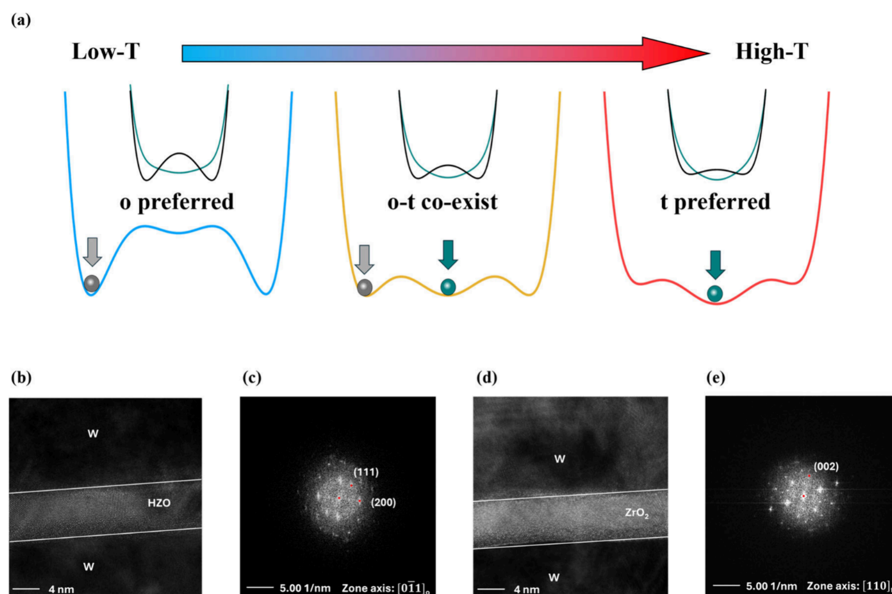

Figure 1. (a) Evolution of the practical L−D energy landscape of HZO as a function of the temperature, assuming a negligible depolarization field. The preferred phase transitions gradually from the o phase to coexistence of o and t phases and eventually to a dominant t phase. (b−e) Cross-sectional HR-TEM images and diffraction pattern of HZO and ZrO_2 thin films. HZO films shows the orthorhombic phase, whereas ZrO_2 films shows the tetragonal phase.

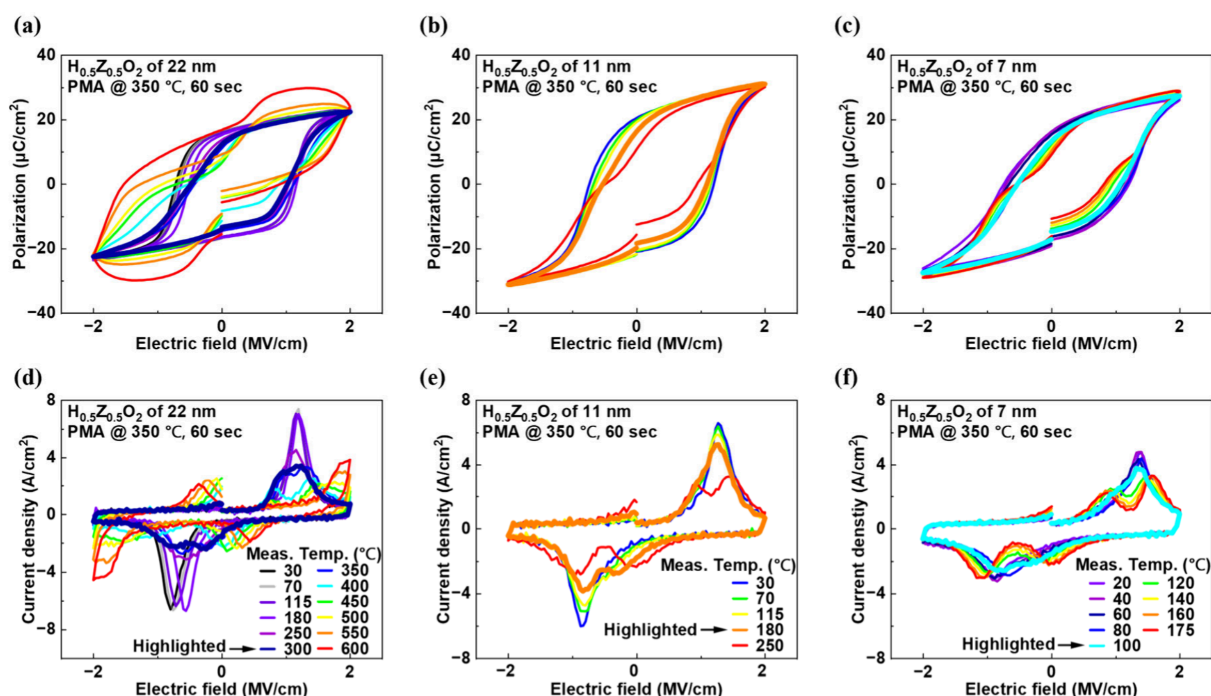

Figure 2. Temperature-dependent experimental data of $H_{0.5}Z_{0.5}O_2$ capacitors with different thickness. (a−c) *P*−*E* hysteresis loops for HZO capacitors with thicknesses of 22, 11, and 7 nm, respectively. All samples exhibit plateaus in the loops, indicative of the phase transition behavior. (d−f) Corresponding *J*−*E* hysteresis loops for the same samples. In each case, a single current density peak gradually splits into two distinct peaks with an increasing temperature. The onset of this splitting, highlighted in the plots, marks the FE−AFE transition temperature for each sample.

As shown in Figure 1b−e, high-resolution transmission electron microscopy (HR-TEM) images and diffraction patterns of HZO and ZrO_2 reveal distinct crystal structures that correlate with their FE and AFE characteristics. However, direct observation of the crystal structure via TEM at elevated temperatures is extremely challenging. To overcome this, we analyzed phase stabilization through temperature-dependent electrical characterization.

In this work, we conduct a comprehensive study on the temperature-dependent phase stability of $Hf_{1-x}Zr_xO_2$ capacitors. By systematically varying the film thickness and composition, we identify the critical conditions that trigger the ferroelectric−antiferroelectric (FE−AFE) transition. Phase-field simulations based on the L−D framework confirm that this transition is driven by stabilization of the t phase at a high temperature. Moreover, we demonstrate that the FE−

https://doi.org/10.1021/acs.nanolett.6c00781
Nano Lett. 2026, 26, 6386−6393

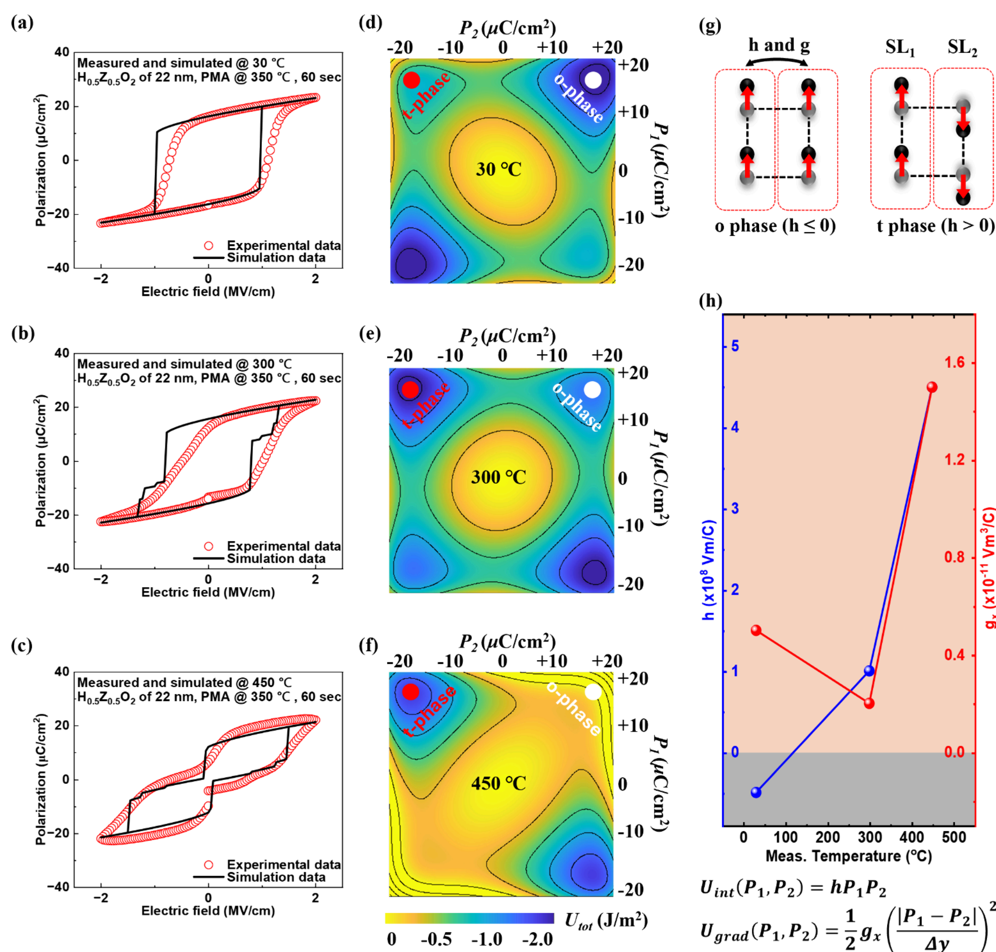

$$U_{int}(P_1, P_2) = hP_1P_2$$

$$U_{grad}(P_1, P_2) = \frac{1}{2}g_x\left(\frac{|P_1 - P_2|}{\Delta y}\right)^2$$

Figure 3. Temperature-dependent simulation results for 22 nm thick $H_{0.5}Z_{0.5}O_2$ capacitors. (a−c) Simulated $P-E$ hysteresis loops at 30, 300, and 450 °C, respectively. Experimental data reflect behavior from large grains with a distribution of transition temperatures, whereas the simulation assumes a single domain with small grains. (d−f) Corresponding 2D energy maps for a single lattice at each temperature, showing that, as the temperature increases, the t phase becomes more thermodynamically stable than the o phase. (g−h) Schematic representations of h and g_x, along with the temperature-dependent evolution of the calibrated values. The sign of h is shown to play a critical role in determining the system's preference for the o or t phase.

AFE transition in HZO is both reversible and repeatable, highlighting its potential for reliable operation in high-temperature electronic systems where stable and repeatable polarization dynamics are critical.

FE−AFE Transition of the $Hf_{0.5}Zr_{0.5}O_2$ Capacitor

Figure 2 presents the polarization−electric field ($P-E$) and current density−electric field ($J-E$) hysteresis loops of HZO capacitors with three different thicknesses. At room temperature, all samples exhibit a clear FE response, characterized by a remanent polarization ($2P_r$) exceeding 30 $\mu C/cm^2$ and two distinct switching current density (J) peaks.

For the 22 nm thick HZO capacitor, as the temperature increases, the maximum polarization (P_{max}) remains nearly unchanged, while the absolute value of the coercive field ($|E_c|$) decreases (Figure 2a and d). This behavior can be explained by the linear relationship between the measurement temperature and coercive field, as demonstrated by Vopsaroiu's model.[23,24] Since this model is only applicable to FE materials, a continuous decrease in $|E_c|$ is observed with an increasing temperature when HZO maintains the FE o phase.

However, above 300 °C, each J peak begins to split into two, accompanied by the appearance of a plateau in the $P-E$ loop, as highlighted in Figure 2a. This behavior marks the onset of t phase stabilization, featuring antiparallel (AP) polarization and inducing a FE−AFE transition through the coexistence of the o and t phases. Consequently, switching between non-zero polarization states is mediated by a stabilized t phase with near-zero net polarization, thereby explaining both the J peak splitting and plateau formation.

At this transitional stage, the polarization does not vanish at a zero electric field, as would be expected for a fully developed AFE response. This is because the system remains in a local energy minimum due to the comparable thermodynamic stabilities of the o and t phases and the presence of an energy barrier that cannot be overcome by thermal energy alone without additional input from the coercive field (E_c).[25] Nevertheless, the partial stabilization of the t phase allows us to define this temperature as the FE−AFE transition temperature.

As the temperature further increases, the dual J peaks become more pronounced and the t phase becomes dominant. Starting from 450 °C, a complete macroscale AFE switching behavior emerges, characterized by switching current density peaks in all four quadrants. Beyond this temperature, all four $|E_c|$ values increase with a further temperature rise. This trend is

https://doi.org/10.1021/acs.nanolett.6c00781
Nano Lett. 2026, 26, 6386−6393

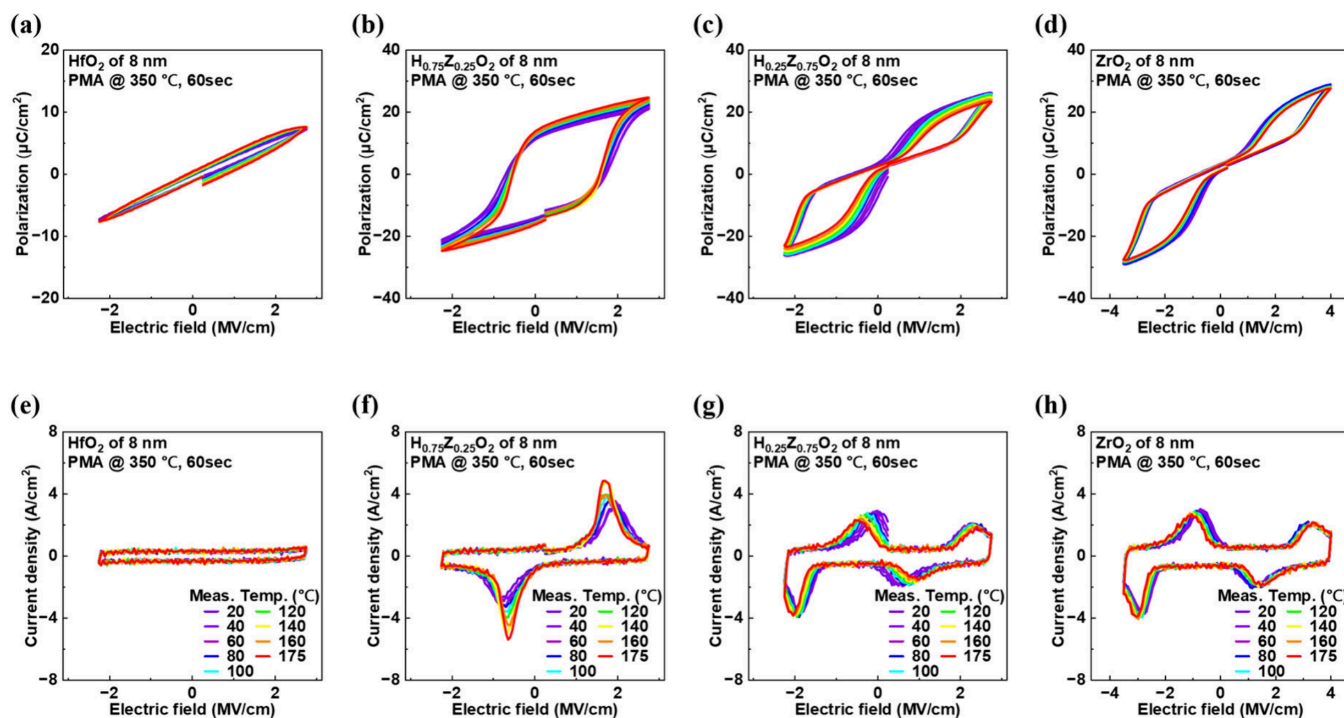

Figure 4. Temperature-dependent experimental results of $H_{1-x}Z_xO_2$ capacitors with a film thickness of 8 nm. (a−d) P−E hysteresis loops for $H_{1-x}Z_xO_2$ capacitors with varying Hf:Zr ratios. (e−h) Corresponding J−E hysteresis loops for the same devices. Among the compositions, only the $H_{0.75}Z_{0.25}O_2$ capacitor exhibits FE behavior at room temperature; however, no clear FE−AFE is observed, and the increase in P_{max} with the temperature is attributed to the relaxation of oxygen vacancies. In contrast, both $H_{0.25}Z_{0.75}O_2$ and ZrO_2 capacitors display AFE behavior at room temperature.

attributed to the increased total free energy, which steepens the L−G energy landscape, resulting in higher $|E_c|$ values.[26−28]

This FE−AFE transition is observed across HZO films of all thicknesses, with the transition temperature strongly dependent on the film thickness. As shown in Figure 2b and e, the transition temperature of 11 nm thick HZO capacitors decreases to as low as 180 °C. Furthermore, in the case of 7 nm thick HZO capacitors, it is further reduced to 120 °C, as shown in Figure 2c and f.

In thinner HZO films, the influence of the highly strained interfacial region between the tungsten (W) electrode and HZO becomes more significant. This interfacial region, associated with lower surface energy, favors the stabilization of a t phase "dead layer", which suppresses the stabilization of the FE o phase.[29] As a result, macroscale stabilization of the t phase and, thus, the FE−AFE transition occurs at lower temperatures.

From this perspective, it can be inferred that the transition temperature could fall below room temperature for even thinner films. Indeed, such behavior is experimentally observed in a 5 nm thick HZO capacitor, as shown in Figure S3.

Simulation Data of a 22 nm $Hf_{0.5}Zr_{0.5}O_2$ Capacitor

To validate the proposed FE−AFE transition model derived from the L−D framework, phase-field simulations were performed using a sublattice phase-field model. This model solves time-dependent Ginzburg−Landau (TDGL) and Poisson's equations to describe the ferroelectric domain dynamics. Within this framework, the dipole−dipole (DD) interaction (h) and the elastic gradient energy coefficient (g_x) account for coupling effects between adjacent sublattices, with details shown in Figure S4.[30]

Figure 3a−c shows the simulated P−E hysteresis loops at 30, 300, and 450 °C. By adjustment of parameters h and g_x with respect to the temperature, the model successfully reproduces the thermally induced FE−AFE transition. Specifically, a FE response is observed at 30 °C, with an intermediate transitional behavior at 300 °C and a well-defined AFE response at 450 °C. This transition is driven by the increasing thermodynamic stability of the t phase at elevated temperatures, as further supported by the temperature dependence of the single-lattice total energy (U_{tot}).[31,32] Although discrepancies exist between experimental and simulated results, primarily because actual devices consist of many grains with a distribution of transition temperatures, while the simulation represents a single domain with a sharp transition, the model still effectively captures the key features of the thermal evolution.

Figure 3d−f presents two-dimensional energy maps of U_{tot} as a function of polarization states P_1 and P_2 at different temperatures. These maps reveal that increasing the temperature raises the energy of the o phase ($P_1 = P_2$) while lowering the energy of the t phase ($P_1 = -P_2$). These simulation results confirm the experimental observation of o and t phase coexistence near 300 °C and support the conclusion that the FE−AFE transition stems from the thermal stabilization of the t phase in a high temperature.

Finally, Figure 3g shows schematic representations of h and g_x, while Figure 3h shows their extracted values across the temperature range. Notably, the DD interaction coefficient h serves as a key indicator of the FE−AFE transition: it switches from negative to positive at the transition temperature, signifying a thermodynamic shift toward antiparallel (AP) polarization between adjacent sublattices ($P_1 = -P_2$). This

https://doi.org/10.1021/acs.nanolett.6c00781
Nano Lett. 2026, 26, 6386−6393

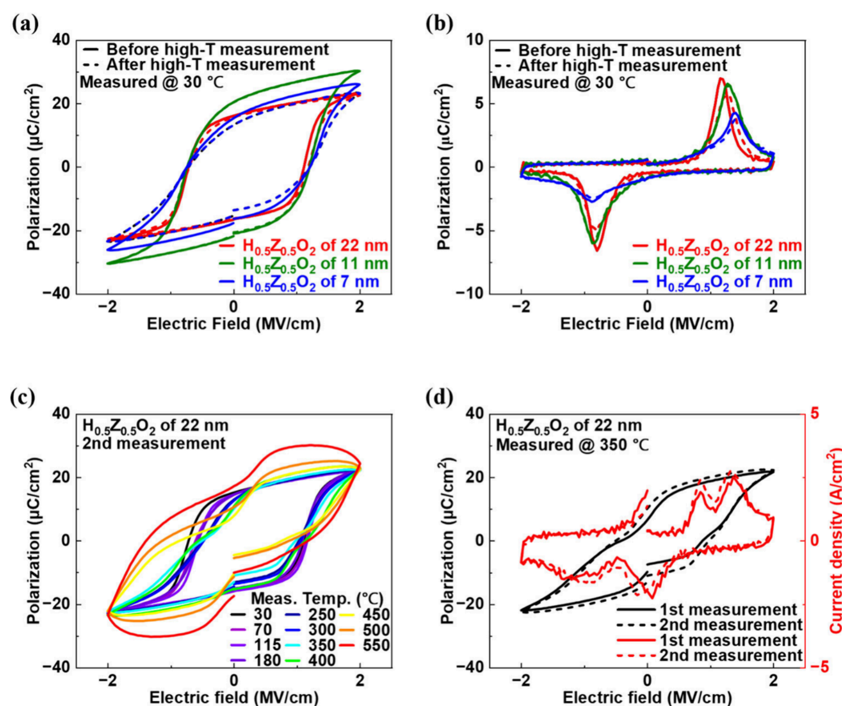

Figure 5. Comparison of experimental *P*−*E* and *J*−*E* hysteresis loops for $H_{0.5}Z_{0.5}O_2$ capacitors of varying thickness before and after high-*T* measurements. (a and b) Only minor differences are observed in the loops before and after heating, indicating that the FE−AFE transition is reversible. (c) The 22 nm thick $H_{0.5}Z_{0.5}O_2$ capacitor was subjected to a second high-temperature cycle, during which the FE−AFE transition was observed again. (d) At 350 °C, the *P*−*E* and *J*−*E* hysteresis loops closely resemble those from the first cycle, demonstrating that the FE−AFE transition is also repeatable.

configuration leads to a negative DD interaction energy (U_{int}), thereby favoring the stabilization of the t phase.

Composition-Dependent Thermal Behavior of $Hf_{1-x}Zr_xO_2$ Capacitors

To examine how composition influences the FE−AFE transition in $Hf_{1-x}Zr_xO_2$ capacitors, we fabricated four capacitors with different Hf:Zr ratios. As shown in Figure 4a and e, the pure HfO_2 capacitor did not exhibit any FE polarization but instead displayed leakage current characteristics at elevated temperatures. In contrast, the pure ZrO_2 capacitor exhibited clear AFE behavior and maintained excellent thermal stability, with only a minimal change in P_{max} even at high temperatures, as shown in Figure 4d and h.

The $Hf_{0.75}Zr_{0.25}O_2$ capacitor demonstrated a well-defined ferroelectric response with a $2P_r$ of 22.5 μC/cm^2 (Figure 4b). However, unlike the 7 nm thick $Hf_{0.5}Zr_{0.5}O_2$ capacitor, it did not show a distinct FE−AFE transition within the same temperature range. Instead, a continuous decrease in the $|E_c|$ value was observed (Figure 4f), consistent with the temperature dependence described in Vopsaroiu's model. Additionally, P_{max} increased with the rising temperature, likely due to the relaxation of oxygen vacancies at an elevated temperature, which stabilize the FE o phase.[33] This effect becomes more significant in thinner films, explaining the notable P_{max} increase observed in the 7 nm thick $H_{0.5}Z_{0.5}O_2$ capacitor. In contrast, for the 11 and 22 nm thick capacitors, the impact of oxygen vacancies is less pronounced, and thus, no clear increase in P_{max} with the temperature is observed.

The absence of a clear FE−AFE transition in the $Hf_{0.75}Zr_{0.25}O_2$ capacitor can be explained on the basis of the L−D model discussed earlier. As the Hf content increases, the energy landscape favors the stabilization of two oppositely polarized states, resulting in deeper global energy minima. Consequently, a higher temperature is required to induce the coexistence of o and t phases necessary for a FE−AFE transition.

In contrast, the $Hf_{0.25}Zr_{0.75}O_2$ capacitor exhibited an AFE response, even at room temperature (Figure 4c). With an increasing temperature, the remaining polarization gradually decreased and approached zero. Simultaneously, $|E_c|$ increased, which can be attributed to the steepening of the L−G energy landscape at higher temperatures (Figure 4g).[26−28] This result suggests that a higher Zr content promotes the stabilization of the t phase at lower temperatures, thereby reducing the FE−AFE transition temperature to below room temperature. This result is consistent with a previous report showing that $Hf_{0.3}Zr_{0.7}O_2$ capacitors exhibit AFE behavior at room temperature but show FE characteristics at 80 K.[10]

Overall, these results demonstrate that composition significantly affects the temperature-dependent phase stability of $Hf_{1-x}Zr_xO_2$. Additional temperature-dependent *P*−*E* hysteresis loops for thicker samples are provided in Figure S5.

Reversible and Repeatable Behavior of the FE−AFE Transition

Finally, the FE−AFE transition in HZO capacitors was found to exhibit both reversible and repeatable behavior. Figure 5a and b shows the room-temperature *P*−*E* and *J*−*E* hysteresis loops of HZO capacitors measured before and after high-temperature measurements. Despite a slight reduction in P_{max}, the FE response remained largely unchanged even after thermal cycling with negligible variation in E_c, demonstrating the reversibility of the FE−AFE transition.

Figure 5c presents the *P*−*E* hysteresis loops from a second high-temperature measurement of the 22 nm thick HZO

capacitor. Although excessive leakage current at 600 °C prevented reliable data acquisition at that temperature, measurements up to 550 °C are successfully obtained. Figure 5d displays the *P*−*E* and *J*−*E* hysteresis loops at 350 °C, where the FE−AFE transition reappeared with only a slight increase in leakage current, confirming the repeatability of the transition during repeated thermal cycling.

In this work, a systematic study of the temperature-dependent behavior of $Hf_{1-x}Zr_xO_2$ capacitors with varying thicknesses and compositions was conducted up to 600 °C. The FE−AFE transition mechanism in HZO was experimentally identified and further validated through sublattice phase-field simulations. Our results show that elevated temperatures promote stabilization of the t phase of HZO, thereby driving the FE−AFE transition. Moreover, scaling down the film thickness significantly lowers the transition temperature to as low as 120 °C, within the temperature range highly relevant to CMOS reliability and self-heating concerns.

We also demonstrate that the FE−AFE transition is highly composition-dependent and exhibits both reversible and repeatable behavior under thermal cycling. These findings highlight the critical role of composition and thickness in tuning the phase stability and switching behavior. In particular, Hf-rich compositions and increased film thickness tend to stabilize the FE phase at higher temperatures, whereas Zr-rich compositions shift the transition to lower temperatures, providing a flexible design space depending on device requirements. This work emphasizes the need for co-designing of electrical and thermal reliability in the design of $Hf_{1-x}Zr_xO_2$-based ferroelectric memory devices. This work offers valuable insights into the integration of hafnia ferroelectrics into advanced CMOS technologies and electronics operating in extreme environments.

Methods

Atomic Layer Deposition (ALD) Growth of the $Hf_{1-x}Zr_xO_2$ Capacitor and Device Characterization. A 10 nm thick Al_2O_3 layer was deposited by ALD onto a 90 nm $SiO_2/p^+Si/SiO_2$ substrate. Subsequently, a 40 nm thick bottom electrode of W was deposited by physical vapor deposition (PVD) sputtering. $Hf_{1-x}Zr_xO_2$ films with varying compositions and thicknesses were deposited at 200 °C by plasma-enhanced atomic layer deposition (PEALD). Top electrode patterns, consisting of circular shapes with a 50 μm radius, were defined using an AZ1518 photoresist and a Heidelberg MLA150 maskless aligner. Following patterning, a 40 nm thick W top electrode was deposited via PVD sputtering. Post-metal annealing (PMA) was conducted using a Jipelec rapid thermal annealing (RTA) system at 350 °C in ambient nitrogen (N_2), with varying annealing durations.

High-temperature measurements were performed using a Microxact CPS-50-HT probe station. All measurements were carried out under a vacuum environment (~4 × 10−6 Torr). Electrical characterization was conducted using a Precision Premier II ferroelectric tester.

ASSOCIATED CONTENT

Supporting Information

The Supporting Information is available free of charge at https://pubs.acs.org/doi/10.1021/acs.nanolett.6c00781.

Additional details for the measurement issue, phase-field simulation, coercive field value, and different thicknesses of $Hf_{1-x}Zr_xO_2$ capacitor characterization data (PDF)

AUTHOR INFORMATION

Corresponding Author

Peide D. Ye − *Elmore Family School of Electrical and Computer Engineering and Birck Nanotechnology Center, Purdue University, West Lafayette, Indiana 47907, United States*; orcid.org/0000-0001-8466-9745; Email: yep@purdue.edu

Authors

Kisoo Nam − *Elmore Family School of Electrical and Computer Engineering and Birck Nanotechnology Center, Purdue University, West Lafayette, Indiana 47907, United States*

Zehao Lin − *Elmore Family School of Electrical and Computer Engineering and Birck Nanotechnology Center, Purdue University, West Lafayette, Indiana 47907, United States*

Tae Ryong Kim − *Elmore Family School of Electrical and Computer Engineering, Purdue University, West Lafayette, Indiana 47907, United States*; orcid.org/0009-0004-5687-2374

Chang Niu − *Elmore Family School of Electrical and Computer Engineering and Birck Nanotechnology Center, Purdue University, West Lafayette, Indiana 47907, United States*; orcid.org/0000-0003-3175-7164

Sumi Lee − *Elmore Family School of Electrical and Computer Engineering and Birck Nanotechnology Center, Purdue University, West Lafayette, Indiana 47907, United States*

Shengyao Huang − *Elmore Family School of Electrical and Computer Engineering and Birck Nanotechnology Center, Purdue University, West Lafayette, Indiana 47907, United States*

Juanjuan Lu − *School of Materials Engineering, Purdue University, West Lafayette, Indiana 47907, United States*; orcid.org/0000-0003-4885-8287

Chang Liu − *School of Materials Engineering, Purdue University, West Lafayette, Indiana 47907, United States*; orcid.org/0009-0006-8509-3569

Sumeet K. Gupta − *Elmore Family School of Electrical and Computer Engineering, Purdue University, West Lafayette, Indiana 47907, United States*

Haiyan Wang − *Elmore Family School of Electrical and Computer Engineering and School of Materials Engineering, Purdue University, West Lafayette, Indiana 47907, United States*; orcid.org/0000-0002-7397-1209

Complete contact information is available at: https://pubs.acs.org/10.1021/acs.nanolett.6c00781

Author Contributions

[†]Kisoo Nam and Zehao Lin contributed equally to this work. Peide D. Ye supervised the project. Kisoo Nam and Zehao Lin fabricated the devices and performed the measurements. Kisoo Nam, Zehao Lin, Chang Niu, Sumi Lee, and Shengyao Huang analyzed the data. Tae Ryong Kim conducted simulation under supervision of Sumeet K. Gupta. Juanjuan Lu and Chang Liu performed TEM under supervision of Haiyan Wang. Kisoo Nam and Zehao Lin wrote the manuscript, and all the authors commented on it.

Notes

The authors declare no competing financial interest.

■ ACKNOWLEDGMENTS

Peide D. Ye and Sumeet K. Gupta acknowledge the support from the U.S. National Science Foundation (Award 2402983). Haiyan Wang acknowledges the support from the U.S. National Science Foundation for the microscopy work (DMR-2016453 and DMREF-2323752).

■ REFERENCES

(1) Takasu, H. The Ferroelectric Memory and Its Applications. *J. Electroceram.* **2000**, *4*, 327−338.

(2) Ishiwara, H. Ferroelectric Random Access Memories. *J. Nanosci. Nanotechnol.* **2012**, *12* (10), 7619−7627.

(3) Eshita, T.; Tamura, T.; Arimoto, Y. Ferroelectric Random Access Memory (FRAM) Devices. In *Advances in Non-volatile Memory and Storage Technology*; Nishi, Y., Ed.; Woodhead Publishing: Sawston, U.K., 2014; Chapter 14, pp 434−454, DOI: 10.1533/9780857098092.3.434.

(4) Mikolajick, T.; Slesazeck, S.; Mulaosmanovic, H.; Park, M. H.; Fichtner, S.; Lomenzo, P. D.; Hoffmann, M.; Schröder, U. Next Generation Ferroelectric Materials for Semiconductor Process Integration and Their Applications. *J. Appl. Phys.* **2021**, *129* (10), 100901.

(5) Böscke, T. S.; Müller, J.; Bräuhaus, D.; Schröder, U.; Böttger, U. Ferroelectricity in Hafnium Oxide Thin Films. *Appl. Phys. Lett.* **2011**, *99* (10), 102903.

(6) Müller, S.; Müller, J.; Singh, A.; Riedel, S.; Sundqvist, J.; Schroeder, U.; Mikolajick, T. Incipient Ferroelectricity in Al-Doped HfO_2 Thin Films. *Adv. Funct. Mater.* **2012**, *22* (11), 2412−2417.

(7) Müller, J.; Schröder, U.; Böscke, T. S.; Müller, I.; Böttger, U.; Wilde, L.; Sundqvist, J.; Lemberger, M.; Kücher, P.; Mikolajick, T.; Frey, L. Ferroelectricity in Yttrium-doped Hafnium Oxide. *J. Appl. Phys.* **2011**, *110* (11), 114113.

(8) Müller, J.; Böscke, T. S.; Müller, S.; Yurchuk, E.; Polakowski, P.; Paul, J.; Martin, D.; Svhenk, T.; Khullar, K.; Kersch, A.; Weinreich, W.; Riedel, S.; Seidel, K.; Kumar, A.; Arruda, T. M.; Kalinin, S. V.; Schlösser, T.; Boschke, R.; van Bentum, R.; Schröder, U.; Mikolajick, T. Ferroelectric Hafnium Oxide: A CMOS-compatible and highly scalable approach to future ferroelectric memories. *Proceedings of the 2013 IEEE International Electron Devices Meeting*; Washington, D.C., Dec 9−11, 2013; DOI: 10.1109/IEDM.2013.6724605.

(9) Müller, J.; Böscke, T. S.; Bräuhaus, D.; Schröder, U.; Böttger, U.; Sundqvist, J.; Kücher, P.; Mikolajick, T.; Frey, L. Ferroelectric $Zr_{0.5}Hf_{0.5}O_2$ Thin Films for Nonvolatile Memory Applications. *Appl. Phys. Lett.* **2011**, *99* (11), 112901.

(10) Müller, J.; Böscke, T. S.; Schröder, U.; Müller, S.; Bräuhaus, D.; Böttger, U.; Frey, L.; Mikolajick, T. Ferroelectricity in Simple Binary ZrO_2 and HfO_2. *Nano Lett.* **2012**, *12* (8), 4318−4323.

(11) Suzuki, K.; Sakuma, K.; Yoshimura, Y.; Ichihara, R.; Matsuo, K.; Hagishima, D.; Fujiwara, M.; Saitoh, M. High-Endurance FeFET with Metal-Doped Interfacial Layer for Controlled Charge Trapping and Stabilized Polarization. *Proceedings of the 2023 International Electron Devices Meeting (IEDM)*; San Francisco, CA, Dec 9−13, 2023; DOI: 10.1109/IEDM45741.2023.10413699.

(12) Mukherjee, S.; Bizindavyi, J.; Luo, Y.-C.; Clima, S.; Read, J.; Popovici, M. I.; Xiang, Y.; Bazzazian, N.; Belmonte, A.; Delhougne, R.; Kar, G. S.; Catthoor, F.; Afanas'Ev, V. V.; Yu, S.; Van Houdt, J. Pulse-Based Capacitive Memory Window with High Non-Destructive Read Endurance in Fully BEOL Compatible Ferroelectric Capacitors. *Proceedings of the 2023 International Electron Devices Meeting (IEDM)*; San Francisco, CA, Dec 9−13, 2023; DOI: 10.1109/IEDM45741.2023.10413879.

(13) Das, D.; Park, H.; Wang, Z.; Zhang, C.; Ravindran, P. V.; Park, C.; Afroze, N.; Hsu, P.; Tian, M.; Chen, H.; Chern, W.; Lim, S.; Kim, K.; Kim, K.; Kim, W.; Ha, D.; Yu, S.; Datta, S.; Khan, A. Experimental Demonstration and Modeling of a Ferroelectric Gate Stack with a Tunnel Dielectric Insert for NAND Applications. *Proceedings of the 2023 International Electron Devices Meeting (IEDM)*; San Francisco, CA, Dec 9−13, 2023; DOI: 10.1109/IEDM45741.2023.10413697.

(14) Schroeder, U.; Mittmann, T.; Materano, M.; Lomenzo, P. D.; Edgington, P.; Lee, Y. H.; Alotaibi, M.; West, A. R.; Mikolajick, T.; Kersch, A.; Jones, J. L. Temperature-Dependent Phase Transitions in $Hf_xZr_{1-x}O_2$ Mixed Oxides: Indications of a Proper Ferroelectric Material. *Adv. Electron. Mater.* **2022**, *8* (9), 2200265.

(15) Prakash, O.; Dabhi, C. K.; Chauhan, Y. S.; Amrouch, H. Transistor Self-Heating: The Rising Challenge for Semiconductor Testing. *Proceedings of the 2021 IEEE 39th VLSI Test Symposium (VTS)*; Virtual Event, April 26−28, 2021; DOI: 10.1109/VTS50974.2021.9441002.

(16) Huan, T. D.; Sharma, V.; Rossetti, G. A., Jr.; Ramprasad, R. Pathways toward Ferroelectricity in Hafnia. *Phys. Rev. B* **2014**, *90* (6), 064111.

(17) Batra, R.; Huan, T. D.; Jones, J. L.; Rossetti, G., Jr.; Ramprasad, R. Factors Favoring Ferroelectricity in Hafnia: A Frist-Principles Computational Study. *J. Phys. Chem. C* **2017**, *121* (8), 4139−4145.

(18) Ong, L.; Osman, J.; Tilley, D. R. Landau Theory of Second-Order Phase Transitions in Ferroelectric Films. *Phys. Rev. B* **2001**, *63* (14), 144109.

(19) Clima, S.; Wouters, D. J.; Adelmann, C.; Schenk, T.; Schröder, U.; Jurczak, M.; Pourtois, G. Identification of the Ferroelectric Switching Process and Dopant-Dependent Switching Properties in Orthorhombic HfO_2: A Frist Principles Insight. *Appl. Phys. Lett.* **2014**, *104* (9), 092906.

(20) Wu, J.; Mo, F.; Saraya, T.; Hiramoto, T.; Kobayashi, M. A Frist-Principles Study on Ferroelectric Phase Formation of Si-Doped HfO_2 through Nucleation and Phase Transition in Thermal Process. *Appl. Phys. Lett.* **2020**, *117* (25), 252904.

(21) Zhu, T.; Ma, L.; Deng, S.; Liu, S. Progress in Computational Understanding of Ferroelectric Mechanisms in HfO_2. *npj Comput. Mater.* **2024**, *10*, 188.

(22) Laudadio, E.; Stipa, P.; Pierantoni, L.; Mencarelli, D. Phase Properties of Different HfO_2 Polymorphs: A DFT-Based Study. *Crystals* **2022**, *12* (1), 90.

(23) Vopsaroiu, M.; Blackburn, J.; Cain, M. G.; Weaver, P. M. Thermally Activated Switching Kinetics in Second-Order Phase Transition Ferroelectrics. *Phys. Rev. B* **2010**, *82* (2), 024109.

(24) Chen, H.; Tang, L.; Liu, L.; Chen, Y.; Luo, H.; Yuan, X.; Zhang, D. Temperature Dependent Polarization-Switching Behavior in $Hf_{0.5}Zr_{0.5}O_2$ Ferroelectric Film. *Materialia* **2020**, *14*, 100919.

(25) Qi, Y.; Rabe, K. M. Phase Competition in HfO_2 with Applied Electric Field from First Principles. *Phys. Rev. B* **2020**, *102* (21), 214108.

(26) Park, M. H.; Kim, H. J.; Lee, Y. H.; Kim, Y. J.; Moon, T.; Kim, K. D.; Hyun, S. D.; Hwang, C. S. Two-Step Polarization Switching Mediated by a Nonpolar Intermediate Phase in $Hf_{0.4}Zr_{0.6}O_2$ Thin Films. *Nanoscale* **2016**, *8* (29), 13898−13907.

(27) Kim, K. D.; Lee, Y. H.; Gwon, T.; Kim, Y. J.; Kim, H. J.; Moon, T.; Hyun, S. D.; Park, H. W.; Park, M. H.; Hwang, C. S. Scale-Up and Optimization of HfO_2-ZrO_2 Solid Solution Thin Films for the Electrostatic Supercapacitors. *Nano Energy* **2017**, *39*, 390−399.

(28) Shin, J.; Shin, D. H.; Kim, K. D.; Seo, H.; Ye, K. H.; Jeon, J. W.; Kim, T. K.; Paik, H.; Song, H.; Lee, S. H.; Choi, J.-H.; Hwang, C. S. Reversible Modulation of Critical Electric Fields for a Field-Induced Ferroelectric Effect with Field-Cycling in ZrO_2 Thin Films. *J. Mater. Chem. C* **2024**, *12* (38), 15423−15434.

(29) Oh, S.; Kim, H.; Kashir, A.; Hwang, H. Effect of Dead Layers on the Ferroelectric Property of Ultrathin $HfZrO_x$ Film. *Appl. Phys. Lett.* **2020**, *117* (25), 252906.

(30) Kim, T. R.; Saha, A. K.; Gupta, S. K. Analysis of Polarization Switching in HZO/ZrO_2 (HZZ) Nanolaminates Based on Sub-lattice Phase-field Model. *Proceedings of the IEEE Proceedings of the 81st Device Research Conference*; Santa Barbara, CA, June 25−28, 2023; DOI: 10.1109/DRC58590.2023.10186928.

(31) Saha, A. K.; Grisafe, B.; Datta, S.; Gupta, S. K. Microscopic Crystal Phase Inspired Modeling of Zr Concentration Effects in $Hf_{1-x}Zr_xO_2$ Thin Films. *Proceedings of the 2019 Symposium on VLSI Technology*; Kyoto, Japan, June 9−14, 2019; DOI: 10.23919/VLSIT.2019.8776533.

(32) Ni, K.; Saha, A.; Chakraborty, W.; Ye, H.; Grisafe, B.; Smith, J.; Rayner, G. B.; Gupta, S. K.; Datta, S. Equivalent Oxide Thickness (EOT) Scaling with Hafnium Zirconium Oxide High-κ Dielectric Near Morphotropic Phase Boundary. *Proceedings of the 2019 IEEE International Electron Devices Meeting (IEDM)*; San Francisco, CA, Dec 7−11, 2019; DOI: 10.1109/IEDM19573.2019.8993495.

(33) Zhang, Z.; Wang, C.; Yang, Y.; Miao, X.; Wang, X. Polarization Enhancement in $Hf_{0.5}Zr_{0.5}O_2$ Capacitors Induced by Oxygen Vacancies at Elevated Temperatures. *Appl. Phys. Lett.* **2023**, *122* (15), 152902.

https://doi.org/10.1021/acs.nanolett.6c00781
Nano Lett. 2026, 26, 6386−6393